https://doi.org/10.5194/tc-2020-70
Preprint. Discussion started: 14 May 2020

The Cryosphere Discussions

Winter drainage of surface lakes on the Greenland Ice Sheet from Sentinel-1 SAR Imagery

Corinne Benedek[1] and Ian Willis[1]
[1]University of Cambridge, CB2 1ER, UK
Correspondence: C.L. Benedek (clb90@cam.ac.uk)

Abstract. Surface lakes on the Greenland Ice Sheet play a key role in its surface mass balance, hydrology, and biogeochemistry. They often drain rapidly in the summer via hydrofracture, which immediately delivers lake water to the ice sheet base over timescales of hours to days and then allows melt water to reach the base for the rest of the summer. Rapid lake drainage, therefore, influences subglacial drainage evolution, water pressures, ice flow, biogeochemical activity, and ultimately the delivery of water, sediments and nutrients to the ocean. It is assumed that rapid lake drainage events are confined to the summer, as this is when all observations to date have been made. Here we develop a method to quantify backscatter changes in satellite radar imagery, which we use to document the drainage of six different lakes during three winters in fast flowing parts of the Greenland Ice Sheet. Analysis of optical imagery from before and after the three winters supports the radar-based evidence for winter lake drainage events and also provides estimates of lake drainage volumes, which range between 0.000046 and 0.0202 km^3. For three of the events, optical imagery allows photoclinometry (shape from shading) calculations to be made showing mean vertical collapse of the lake surfaces ranging between 4.04 m and 7.25 m, and drainage volumes of 0.004 km^3 to 0.049 km^3. The findings show that background winter ice motion can trigger rapid lake drainage, which may have important implications for subglacial hydrology and biogeochemical processes.

1 Introduction

Lakes form each summer on the surface of the Greenland Ice Sheet (GrIS), particularly in the upper ablation and lower accumulation areas (McMillan et al., 2007; Selmes et al., 2011; Liang et al., 2012; Pope et al., 2016; Williamson et al., 2017). They enhance melt rates via their effects on albedo (Lüthje et al., 2006; Tedesco et al., 2012), store water and delay its delivery to the ocean (Banwell et al., 2012; Leeson et al., 2012; Arnold et al., 2014), and collect nutrients - the products of surface inorganic and organic chemical processes (Musilova et al., 2017; Lamarche-Gagnon et al., 2019). Many lakes drain over the summer (Selmes et al., 2013; Williamson et al., 2017), sometimes slowly by overtopping their basins and incising a channel (Hoffman et al., 2011; Tedesco et al., 2013; Koziol et al., 2017) but often rapidly by hydrofracturing from the surface to the base of the ice sheet (Das et al., 2008; Doyle et al., 2013; Tedesco et al., 2013; Stevens et al., 2015; Chudley et al., 2019). The rapid drainage of a lake may trigger the opening of crevasses and the generation of moulins (Hoffman et al., 2018) or the drainage of other lakes (Christoffersen et al., 2018) through ice dynamic coupling. Rapid lake drainage provides a major shock to the ice sheet as millions of cubic metres of water are delivered to the bed in a few hours, and the resultant fracture

https://doi.org/10.5194/tc-2020-70
Preprint. Discussion started: 14 May 2020

permits meltwater to reach the bed for the rest of the summer. This generates a radiating subglacial water 'blister' beneath the draining lake, which evolves into a conduit in the down-glacier direction allowing the lake water and subsequent melt water to be evacuated (Pimentel and Flowers, 2010; Tsai and Rice, 2010; Dow et al., 2015). High water pressures are generated transiently during lake drainage (Banwell et al., 2016), lifting the ice sheet off the bed and increasing temporarily its sliding velocity (Das et al., 2008; Doyle et al., 2013; Tedesco et al., 2013; Stevens et al., 2015; Chudley et al., 2019). The subsequent evolution of the subglacial conduit may lower water pressures (Schoof, 2010; Hewitt, 2013; Werder et al., 2013; Banwell et al., 2016) and reduce sliding speeds (Bartholomew et al., 2010).

Rapid lake drainage and subsequent meltwater influx also alter subglacial biogeochemistry as large volumes of oxygenated water containing surface microbial taxa and inorganic and organic nutrients replace wintertime anoxic waters and associated microbes, shifting subglacial redox potential and associated biogeochemical pathways (Wadham et al., 2010; Shade et al., 2012). Lake drainage events, therefore, ultimately control the quantity and quality of water issuing from the ice sheet. They can produce small floods that flush out sediments (Bartholomew et al., 2011), raise levels of phosphorus, nitrogen and sulphate (Hawkings et al., 2016; Wadham et al., 2016), and mark a transition from net subglacial methane production and proglacial export during winter to consumption with little or no export in the summer (Dieser et al., 2014).

Much of what we know about the locations, timings and magnitudes of rapid lake drainage events comes from the analysis of optical satellite imagery (Box and Ski, 2007; McMillan et al., 2007; Sneed and Hamilton, 2007; Leeson et al., 2013; Moussavi et al., 2016; Pope et al., 2016; Williamson et al., 2018) although studies have recently begun using optical imagery from drones (Chudley et al., 2019), and airborne and satellite radar data (Koenig et al., 2015; Miles et al., 2017). Conventional understanding is that rapid lake drainages are confined to the summer. They may be driven by active in-situ hydrofracture through the lake bottom triggered by rising water levels in the lake (Alley et al., 2005; van der Veen, 2007; Krawczynski et al., 2009; Arnold et al., 2014; Clason et al., 2015) and/or by passive fracture in response to perturbations in ice sheet flow induced by surface meltwater initially tapping the bed via nearby moulins (Stevens et al., 2015; Chudley et al., 2019). Conventional understanding is that lakes that completely or partially drain during the summer then freeze during the winter, opening of crevasses and the generation of moulins maintaining a liquid water core (Selmes et al., 2013; Koenig et al., 2015; Miles et al., 2017; Law et al., forthcoming 2020). High proglacial stream discharge anomalies outside of the summer melt season have been attributed to the release of stored water from the ice sheet. Evidence from one study showed that water was released from englacial or subglacial water stores (Rennermalm et al., 2012) although the formation of surface collapse features reported in another, suggested water has the potential to be released from surface lakes during the winter (Russell, 1993).

Here we develop an algorithm to carefully examine spatial and temporal variations in microwave backscatter in Sentinel-1 satellite synthetic aperture radar (SAR) imagery to document the location and timing of six separate lake drainage events over three different winters. We confirm the winter lake drainages and provide estimates of draining lake volumes through calculation of water areas and depths in Landsat-8 optical imagery from the previous and subsequent melt seasons. For three of the events, the optical imagery allows us to calculate surface elevation change s associated with the lake drainages using the technique of photoclinometry.

https://doi.org/10.5194/tc-2020-70
Preprint. Discussion started: 14 May 2020

The Cryosphere Discussions
Open Access
EGU

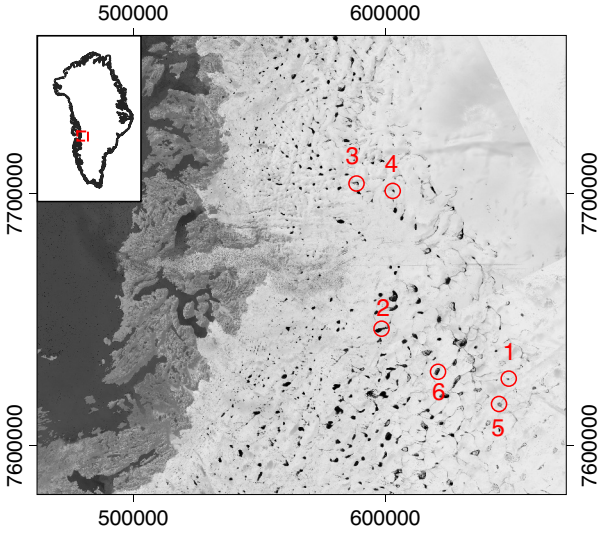

Figure 1. Study area within the context of the Greenland Ice Sheet (inset). Distribution of all surface lakes detected from optical imagery, with the six winter draining lakes highlighted (red numbers, in chronological order of drainage), which are shown in more detail in Figure 6. The base map is a composite image showing the maximum $NDWI_{ice}$ observed for each pixel in Landsat-8 optical images over the course of all summers from 2014 through 2017. The outline of Greenland is from OpenStreetMap (© OpenStreetMap contributors 2019. Distributed under a Creative Commons BY-SA License.)

2 Methods

The study was conducted over a 30,452 km^2 area of the GrIS (Figure 1). The site spans elevations from 300 meters to 2038 meters above sea level and includes approximately 300 lakes over 5 pixels in size (0.0045 km^2). The study period spans imagery from July 2014 to May 2017 and includes, therefore, three fall-winter-spring periods from October through May, hereafter "winter periods": 2014/15, 2015/16 and 2016/17.

There are five components to our analysis. First, a lake mask is established from optical imagery. Second, for each lake, trends in mean backscatter change during the winter are calculated. Third, the backscatter changes are used to identify large anomalous, sudden and sustained increases in backscatter that are indicative of winter lake drainage events. Fourth, optical images from before the winter periods are used to provide estimates of lake volumes prior to drainage. Fifth, for three of the events, optical imagery and the technique of photoclinometry are used to calculate patterns of surface elevation change associated with the lake drainage events, providing independent estimates of lake drainage volumes. These components to our analysis are described more fully below.

https://doi.org/10.5194/tc-2020-70
Preprint. Discussion started: 14 May 2020

2.1 Establishing lake outlines using optical imagery

Prior to each winter, lake boundaries were delineated based on a calculation of maximum $NDWI_{ice}$ per pixel from optical imagery during the preceding late melt season (late July through August). Landsat-8 Tier 1 TOA images were chosen based on minimal cloudiness (filtered using the Landsat-8 QA band) and images were removed from the set manually where cloudiness interfered with $NDWI_{ice}$ calculations. Late season images were chosen so that lakes that had already drained prior to the end of summer freeze-over period were not included in the calculations. For each late summer period, multiple images were needed to cover the entire region and to obtain at least one cloud-free pre-freeze-over image for all areas of the study site.

Normalized Difference Water Index $NDWI_{ice}$ was calculated for each pixel in each of the images in the Landsat-8 set (Yang and Smith, 2012) (Equation 1).

$$NDWI_{\text{ice}} = (Blue–Red)/(Blue + Red) \quad (1)$$

where Blue and Red refer to band reflectance.

For each late summer, a mask was created from the set of Landsat-8 images by recording the maximum $NDWI_{ice}$ value observed in each pixel over the set and setting an $NDWI_{ice}$ threshold of 0.25 following Yang and Smith (2012) and Miles et al. (2017) indicating the presence of deep water. These lake masks, one for each summer, were then used as the basis for defining lake boundaries for the analysis of backscatter changes in SAR imagery during the subsequent winter periods.

2.2 Calculating time series of mean lake backscatter from SAR imagery

For each winter period, lake masks delineated from the previous late summer's Landsat-8 images were applied to Sentinel-1 SAR images in order to calculate trends in mean backscatter for each lake over time. Changes in mean backscatter of each lake were tracked over each winter period and these changes were used to identify wintertime lake drainages as described further below.

Google Earth Engine (Gorelick et al., 2017) was used to select a series of Sentinel-1 images over the study site. Sentinel-1 files on the Google Earth Engine repository have been pre-processed using the following steps: i) Apply Orbit File; ii) Thermal Noise Removal; iii) Radiometric Calibration (to Gamma Nought); iv) Terrain Correction (using SRTM, to UTM 22 projection). We restricted our selection to ascending relative orbits to reduce backscatter variation from image to image due to look angle alone. While Sentinel-1 has a repeat pass time of 12 days per satellite (6 days when both 1A and 1B satellites are combined), not all images are collected, sometimes leaving lengthy data gaps over the study site. For the purposes of this study, images from ascending Relative Orbit 17 were used as this orbit provided the greatest number of images over the study site within the study period. Three images were removed as outliers as they exhibited significant scene-wide departures from the backscatter of images adjacent in time. Both HH and HV polarizations are available for our study site, but we include only the data from the HV polarization as it more clearly shows buried shallow near-surface lakes (Miles et al., 2017).

https://doi.org/10.5194/tc-2020-70
Preprint. Discussion started: 14 May 2020

2.3 Isolating drainage events

For each winter, the mean backscatter of each lake was calculated for each Sentinel-1 image to create a time series of mean backscatter for each lake. Lakes over the winter undergo a slow freeze-through process (Selmes et al., 2013; Law et al., forthcoming 2020). We hypothesize, therefore, that a winter lake drainage event would appear as a sudden increase in backscatter between two images, which is then maintained over a long period of time, in much the same way as it does for a summer lake drainage (Miles et al., 2017). To be certain that a large increase in mean backscatter is an expression of a change in a particular lake, rather than an artifact of the sensing process, an anomalous large increase in lake backscatter is identified by comparing the backscatter change of each lake to that for all the other lakes in the scene in the same consecutive image pair. For each consecutive image pair, the z-score of backscatter change for each lake is calculated relative to the backscatter change of all lakes across the scene and a threshold of +1.5 is used to isolate those lakes that experience a greater than average increase in backscatter between images. Change events were then filtered based on the time between consecutive images.

To be sure that a large anomalous and sudden increase in backscatter was sustained rather than just an isolated variance, filters were employed to check for reversal in the subsequent three images, where those images occurred within 48 days of the originals. In each timestep, lakes were removed from consideration if the reversed backscatter change was greater than 25% of the magnitude of the original anomalous increase (see 'A' in Figure 2). Lakes were also checked to be sure that there was no preceding dip that was being reversed by the anomalous increase itself (see 'C' in Figure 2). The aim of this processing was to identify lakes that showed a sustained backscatter step change increase between two relatively stable levels. Given that there are some large gaps in Sentinel-1 data collection within each relative orbit, specifying that a change event had to occur within 12 days and be sustained for up to 48 days, reduced the number of events compared to those originally detected. Finally, only lakes greater than 5 pixels in size were considered.

2.4 Lake volume

Lake depths were calculated from Landsat 8 imagery using physical principles based on the Bouguer-Lambert-Beer law as outlined elsewhere (Sneed and Hamilton, 2007; Pope et al., 2016; Williamson et al., 2018). For the six lakes that drained in the winter, Landsat-8 images showing the greatest lake area from the melt season prior to the lake drainage event were selected manually. Lake depth, z, was calculated on a per-pixel basis from:

$$z = [ln(Ad - Rinf) – ln(Rpix - Rinf)]/g \quad (2)$$

where A_d is the lake bottom albedo, Rinf is the reflectance of a deep water pixel, Rpix is the reflectance of the pixel being assessed, and g is based on calibrated values for Landsat 8 (Pope et al., 2016). For this analysis, calculations were performed for both the red and panchromatic bands with the final depths averaged between the two results (Pope et al., 2016; Williamson et al., 2018). For each band, the outline of each lake was established using a mask based on an $NDWI_{ice}$ threshold of 0.25. The reflectance values of all pixels immediately exterior (30m) to this outline were averaged to obtain a value for A_d. Reflectance

https://doi.org/10.5194/tc-2020-70
Preprint. Discussion started: 14 May 2020

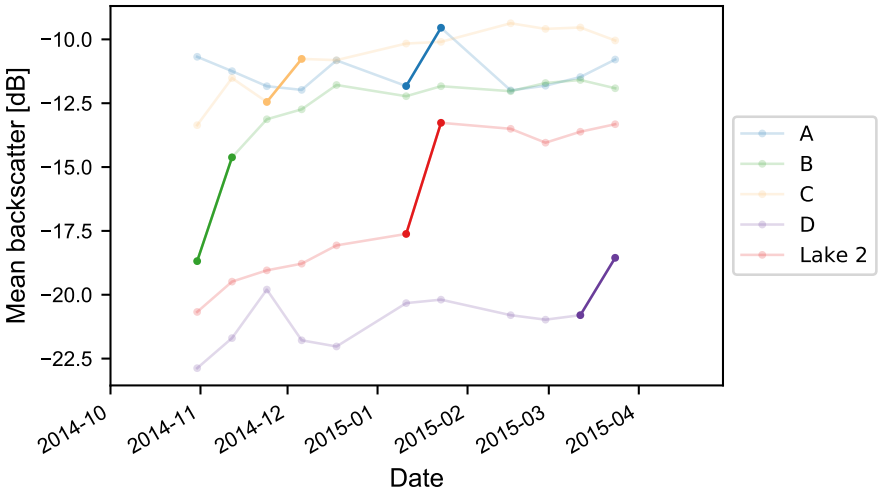

Figure 2. This figure illustrates the filtering criteria for identifying drained lakes. (A) Anomalous sustained step change but one that is not sustained. (B) Anomalous increase but with insufficient history to determine if the change was an adjustment from a previous dip or step increase from a previous low. (C) Anomalous sustained change but with a prior dip such that this change was a return to prior values rather than a sustained change. (D) Anomalous change without sufficient information to confirm a sustained change. Lake 2 shows anomalous sudden and sustained backscatter change depicting lake drainage. All the time series shown are results from actual lakes in the 2014-2015 season. Bold line segments are the transitions that met the z-score threshold.

of deep water was determined per image by selecting the darkest pixel in each image. For each lake, the depths of all lake pixels were added to calculate lake volume.

2.5 Photoclinometry

This technique is also known as 'shape-from-shading' and uses a single surface DEM, and a series of optical satellite images to calculate surface slopes, elevations, and therefore elevation changes. We used the ArcticDEM (5m resolution mosaic) for the part of the ice sheet encompassing the draining lakes, which we resampled using bilinear interpolation to match the 30m Landsat-8 resolution. We used Landsat-8 images from before and after each of the six winter lake drainage events. Image pairs were chosen to be as close to the timing of each lake drainage as possible, but also to be cloud free over the lake, and to be from the same Path and Row across each pair to reduce any incidence angle error. It was also important to find image pairs that contained snow cover in order to produce clear relationships between reflectance and slope angle that could be used to determine slopes and therefore elevations across the lakes. The calculations follow the methods outlined by Pope et al. (2013) and were completed for three of the six drained lakes as suitable Landsat-8 image pairs did not exist for the other three.

For each image (six in total, two per lake) the following procedure was adopted. Band 4 was extracted and used as the basis for calculation. Transects were drawn across the lake parallel with the solar azimuth at the time of the image. Transects were

https://doi.org/10.5194/tc-2020-70
Preprint. Discussion started: 14 May 2020

10 km in length, to achieve sufficient coverage of both the lake and ambient area, and were spaced 250 m apart across the width of the lake. The lake was outlined manually based on the Band 4 image, and a 100m buffer external to the lake boundary was added to ensure that the changing lake topography was not included in the production of a baseline relationship between topography and reflectance. Each transect was sampled every 30m along its length for Band 4 reflectance, for topography in the ArcticDEM, and for the binary delineation of buffered lake area or ambient area. Sample lake imagery is shown in Appendix B. Surface slope was calculated along each transect from the elevation difference between adjacent nodes. A linear relationship was established between slope and Band 4 reflectance for all pixels outside the buffered lake area.

For each image processed, the linear slope-reflectance relationship established for non-lake pixels was then applied to the buffered lake pixels to calculate slope for each of the nodes on each transect across the buffered lake area. Elevation for each node on each transect across the buffered lake was reconstructed by integrating the slope values, starting from the known elevation of the node at the edge of the buffered lake on the north side of the lake and progressing to the south side. This resulted in small offset errors on each transect at the nodes on the south side of the buffered lake, where elevations did not match the known elevations from the DEM. These offsets were closed by linearly tilting each transect across the buffered lake, adjusting all elevations accordingly. Elevation values were then interpolated (IDW method) using a 250 m x 30 m grid to create a digital elevation model of each lake before and after drainage. These grids were then differenced to calculate the patterns of lake surface elevation change due to winter lake drainage.

3 Results

3.1 Winter lake drainage from Sentinel-1 imagery

We found six lakes that experienced large, anomalous, sudden and sustained backscatter increases that we interpret as lake drainage events over the three winter seasons analyzed. The lake locations are shown in Figure 1 and the drainage characteristics are summarized in Table 1. Although one of the criteria for lake selection was having a z-score of backscatter increase greater than 1.5, results show that all six lakes that met all of the criteria had a z-score of backscatter increase greater than 2.0 (Table 1). The size of the drained lakes varied widely (between 0.18km^2 and 6.84 km^2) as did the timing of drainage within the winter season, ranging between early November and late February (Table 1). During the 2015-2016 winter, Lakes 3 and 4 towards the north of the study area, and separated by a straight-line distance of 14.9 km, drained within the same 12 day time period (Figure 1 and Table 1). Lake volumes vary between 0.000046 km^3 and 0.0202 km^3. These may be underestimations of drained volume as physically based depth calculations can underestimate the depth of deep water (Pope et al., 2016; Williamson et al., 2018) and as the lake may have continued to fill after the last available Landsat-8 image. Conversely, they may be slight overestimations of drained volume if some water froze prior to drainage.

For each lake the backscatter changes signifying a drainage are shown in Figure 3. All lakes generally undergo a large, anomalous, sudden change from predominantly dark (low backscatter) to light (higher backscatter) when compared to their surroundings. This transition is visually more obvious for the larger lakes (Lakes 1, 2, 5, and 6) and less clear for the smaller

https://doi.org/10.5194/tc-2020-70
Preprint. Discussion started: 14 May 2020


The Cryosphere Discussions

Table 1. Details of the lake drainage events. Location refers to longitude, latitude (WGS84). The drainage dates are the Sentinel-1 image dates over which the anomalous change was identified. The delta dB is the mean change in backscatter (measured in decibels) within the lake boundary from one image to the next. The z-score is the measure of the magnitude of this backscatter change compared to the backscatter change of other lakes in the study site across the same image pair. Lake area is the size of the lake delineated by the $NDWI_{ice}$-based mask. Lake volume was calculated as described in Methods.

Lake	Location	Drainage Date	delta dB	z-score	Pre-drainage Lake Area	Pre-drainage Mean Lake Depth	Pre-drainage Lake Volume
Lake 1	-47.32 , 68.70	11 Nov 2014 to 23 Nov 2014	-4.3	3.5	0.18 km^2	0.50 m	0.000046 km^3
Lake 2	-48.52, 68.91	10 Jan 2015 to 22 Jan 2015	-4.4	3.4	6.84 km^2	3.20 m	0.0202 km^3
Lake 3	-48.75, 69.43	05 Jan 2016 to 17 Jan 2016	-3.8	2.7	0.93 km^2	1.43 m	0.0011 km^3
Lake 4	-48.38, 69.40	05 Jan 2016 to 17 Jan 2016	-2.3	2.6	0.71 km^2	2.32 m	0.0014 km^3
Lake 5	-47.43, 68.62	10 Feb 2016 to 22 Feb 2016	-3.2	2.8	1.43 km^2	0.82 m	0.0017 km^3
Lake 6	-48.03, 68.75	06 Nov 2016 to 18 Nov 2016	-9.3	2.2	2.86 km^2	1.33 m	0.0032 km^3

lakes (Lakes 3 and 4) (Figure 3) although the mean backscatter change for Lake 3 is actually slightly greater than that for Lake 5 (Table 1).

The mean backscatter time series for each lake is shown in Figure 4. Each series shows at least two dates of similar backscatter values prior to the step change from low to high backscatter. Each series maintains its higher backscatter after the initial jump. The backscatter changes of Lakes 3 and 4 are smaller in dB than the change that occurs in Lake 6 but the z-scores signifying how unusual the jumps are when compared to those in other lakes, are significantly higher in Lakes 3 and 4 (Table 1).

Drained lakes are filtered out based on their large anomalous increases in backscatter in comparison with other lakes, that occur within 12 days, and that are sustained for at least 48 days. All other lakes undergo changes in backscatter that are comparable with those in nearby lakes, or they experience large anomalous backscatter changes but that are not sustained. Figure 5 shows the mean backscatter of Lake 6 over time together with that for the 10 largest lakes in its immediate vicinity (within a 20 km x 20 km square, centered on Lake 6). The sudden increase in mean backscatter of Lake 6 is far greater than that for the surrounding lakes. Lake 6 initially has low backscatter that is comparable with that for some of the surrounding lakes. Optical imagery from the end of the previous summer shows Lake 6 and these other 'low backscatter lakes' were water filled. Over a single image transition, Lake 6 experiences a backscatter increase to levels that are comparable with other surrounding lakes that optical imagery from the end of the previous summer showed were drained. The lakes surrounding Lake 6 experience much slower backscatter increases over time, which we interpret to be slow freezing of the water in the filled lakes or the ice surface in the bottom of the drained lakes. Figure 5 also illustrates what the backscatter changes look like within the Sentinel-1 imagery. Small changes are observable within the surrounding lakes but a much bigger change is seen in Lake 6.

https://doi.org/10.5194/tc-2020-70
Preprint. Discussion started: 14 May 2020

The Cryosphere
Discussions
Open Access
EGU

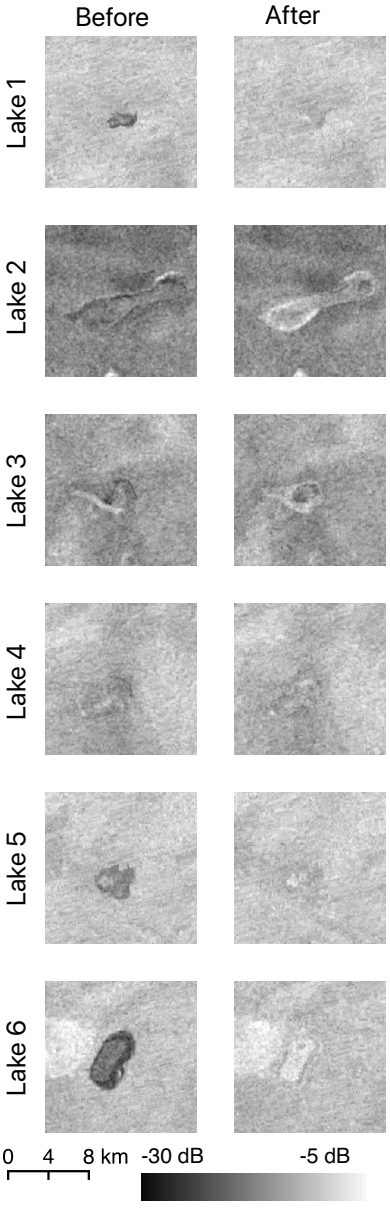

Figure 3. Sentinel-1 backscatter for each lake immediately before and after drainage. Before and after drainage dates are listed in Table 1. Note the lakes before drainage have a lower backscatter that changes to a higher backscatter across the image pair. Connective lines are omitted from the graph when the time between images is greater than 12 days.

https://doi.org/10.5194/tc-2020-70
Preprint. Discussion started: 14 May 2020

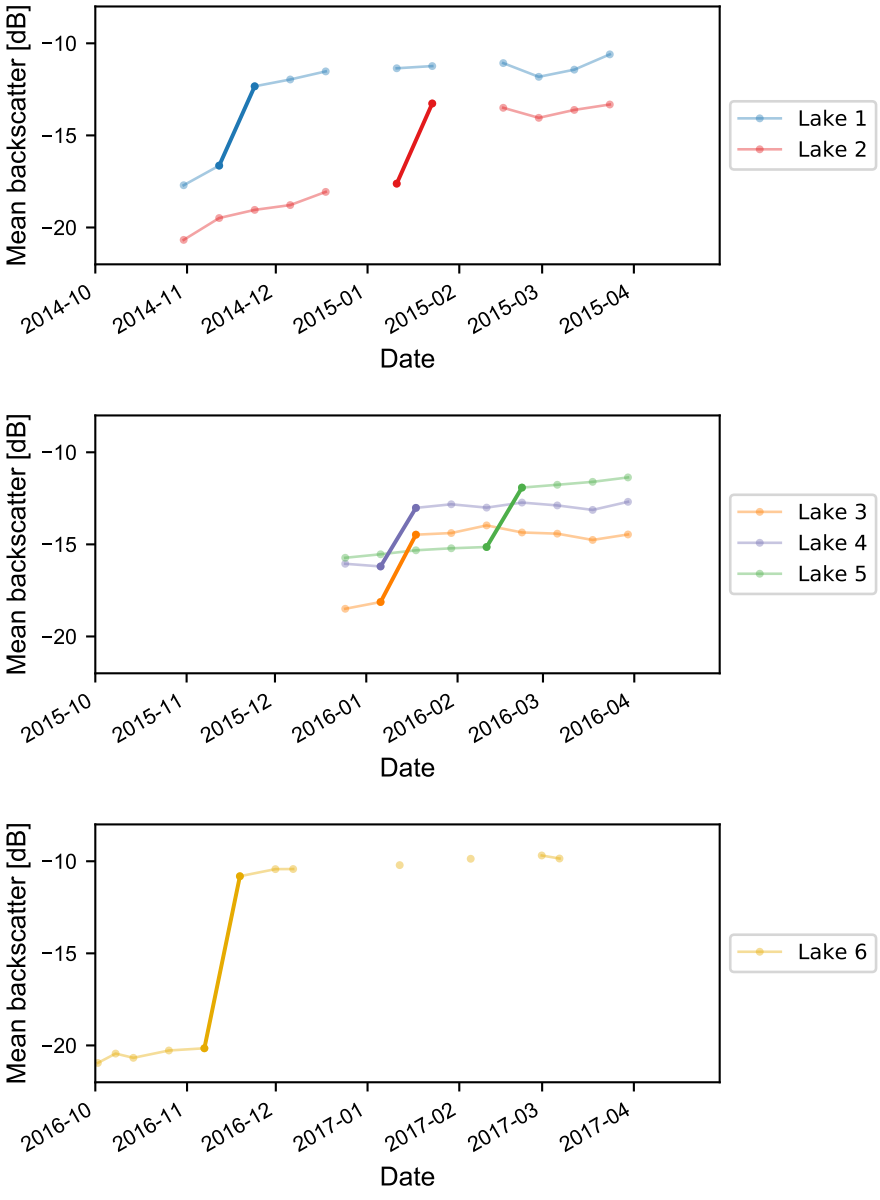

Figure 4. This figure shows the backscatter time series for the lakes with identified drainage events. Connecting lines are only included when time between images is 12 days or less. Each series represents one lake and each point the mean backscatter of all of the lake's pixels in a particular Sentinel-1 image. Bold lines indicate the transition determined to be the drainage event.

3.2 Confirmation by optical imagery

Analysis of Landsat-8 imagery from the summers prior and subsequent to the six inferred winter drainage events supports the interpretation that the changing SAR backscatter represents lake drainage. Using the same method described above for

https://doi.org/10.5194/tc-2020-70
Preprint. Discussion started: 14 May 2020

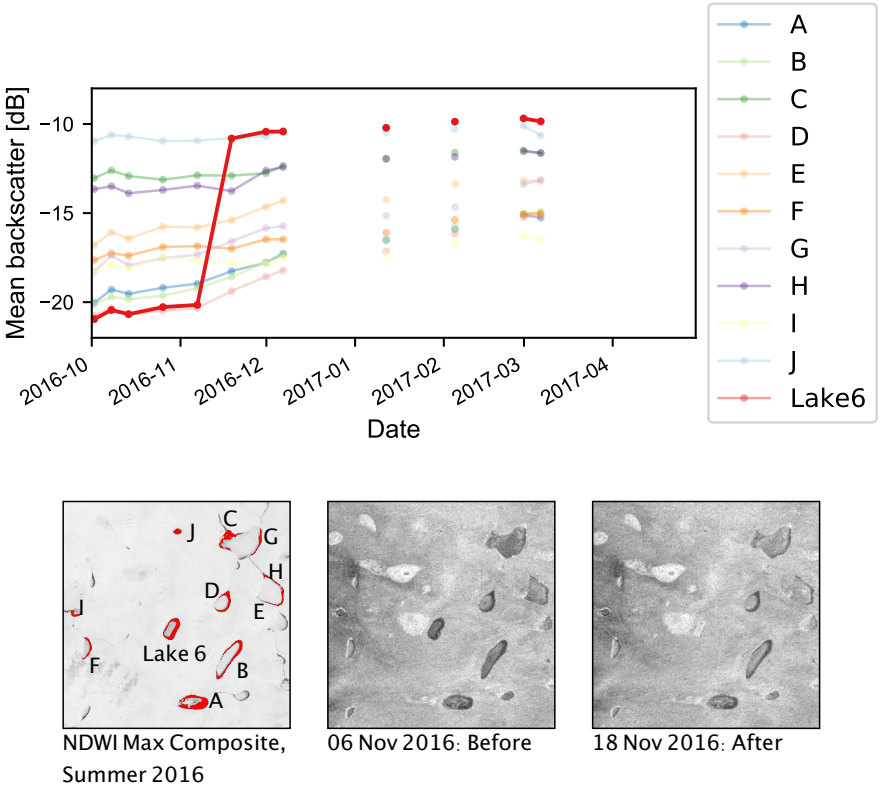

Figure 5. Sentinel-1 backscatter time series for the largest 10 lakes within 20 km of Lake 6. Image (a) is a composite maximum $NDWI_{ice}$ image for late summer 2016, prior to lake drainage showing the lakes included in the graph above. Images (b) and (c) are Sentinel-1 backscatter images for 06 November 2016 and 18 November 2016 across which the drainage of Lake 6 is observed. Connective lines are omitted from the time series graph when the time between images is greater than 12 days. While the backscatter of the surrounding lakes undergoes some gradual increase over time, the backscatter increase of Lake 6 is much greater than that seen in the other lakes.

creating composite $NDWI_{ice}$ masks for late summer (from late July and August images), here we create similar $NDWI_{ice}$ masks for each summer but using all cloud-free Landsat-8 images between May and August from 2014 to 2017. The purpose of this is to calculate maximum lake areas for all lakes, including the six lakes inferred to drain during the winter, in the summers prior and subsequent to the winter lake drainages. Maximum summer water coverages for the six winter draining lakes are shown in Table 2. The corresponding composite $NDWI_{ice}$ images for each summer are shown in Figure 6.

The maximum lake extents for Lakes 1, 2, 5 and 6, appear larger in the summers prior to drainage than after drainage. This suggests that the winter lake drainages were associated with fractures / moulins that remained open, allowing the following summers' meltwater reaching the basin to drain directly into the ice sheet. These reductions in maximum lake extents contrast with those observed for the many surrounding lakes, which fill to around the same size in the adjacent summers. Lakes 3 and 4 show little difference in area before and after drainage, but the lakes do change shape (Figure 6). This suggests that the fractures

https://doi.org/10.5194/tc-2020-70
Preprint. Discussion started: 14 May 2020

Table 2. Maximum lake area for each summer generated by calculating maximum $NDWI_{ice}$ per pixel from May through August each year. The lake $NDWI_{ice}$ threshold is set at 0.25 and area is calculated based on all pixels in the lake above this value.

	Lake Areas (km^2)			
Lake	Summer 2014	Summer 2015	Summer 2016	Summer 2017
Lake 1	0.0936*	0.0189	0.4734	0 (cloud cover)
Lake 2	6.498*	0.936	2.774	3.595
Lake 3	0.967	0.934*	1.532	0.698
Lake 4	0.699	0.639*	0.658	0.495
Lake 5	0.166	2.201*	0.471	0 (cloud cover)
Lake 6	1.001	1.987	2.757*	0.614

* indicates pre-drainage area.

/ moulins associated with the winter drainage of these lakes closed shut or were advected out of the lake basins, allowing the lakes to form again in the subsequent summer. Lakes that experience large area changes recover their area over time, but not necessarily within the first summer following drainage.

Finally, we use the technique of photoclinometry based on the 5 m ArcticDEM mosaic and Landsat-8 imagery (Table S2) before and after the winter drainage events (see Methods) to calculate surface elevation changes across three of the lakes (Figure 7). Landsat-8 images suggest a smooth flat surface to each lake prior to drainage and a rough topography following drainage, suggesting the caving in of a frozen, snow-covered lake surface during drainage. Mean elevation changes calculated from photoclinometry using these images are 7.25 m for Lake 2, 1.21 m for Lake 5, and 4.04 m for Lake 6. These depths are greater than those calculated based on the last available optical image, seen in Table 1 but are internally consistent in their rank from smallest to largest. The per-pixel elevation changes provide independent estimates of drainage volumes for Lakes 2, 5 and 6 of 0.049 km^3, 0.004 km^3 and 0.018 km^3 respectively. In relative terms, these compare well with the volume changes estimated from $NDWI_{ice}$ areas and pixel depths, but are 2 – 3 times larger for Lakes 2 and 5 and over 5 times larger for Lake 6.

3.3 Discussion

We have developed a novel algorithm for analysis of Sentinel-1 SAR imagery and used it to identify six winter lake drainage events on the GrIS, the first such events to be reported in full. Because SAR backscatter is often difficult to interpret (White et al., 2015) we have validated our technique by examining Landsat-8 optical imagery from the previous and subsequent summers. Changes in lake area and volume as well as topographic changes expressed through photoclinometry support the inference that these large, anomalous, sudden and sustained backscatter increases are lake drainage events.

https://doi.org/10.5194/tc-2020-70
Preprint. Discussion started: 14 May 2020

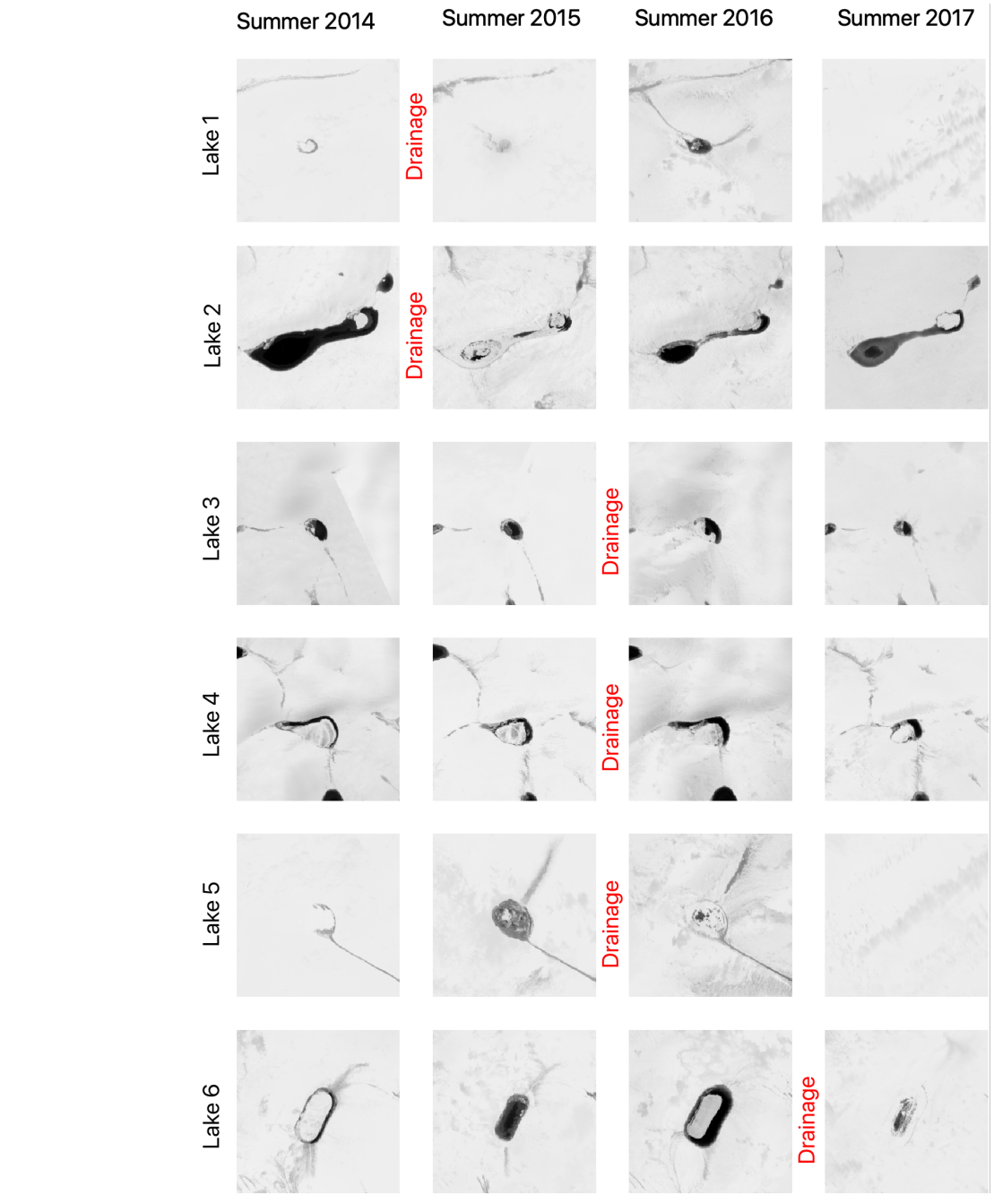

Figure 6. $NDWI_{ice}$ for each identified drained lake at the peak of each summer within the study. Note that most lakes take more than a single summer season to recover from their winter drainage.

https://doi.org/10.5194/tc-2020-70
Preprint. Discussion started: 14 May 2020

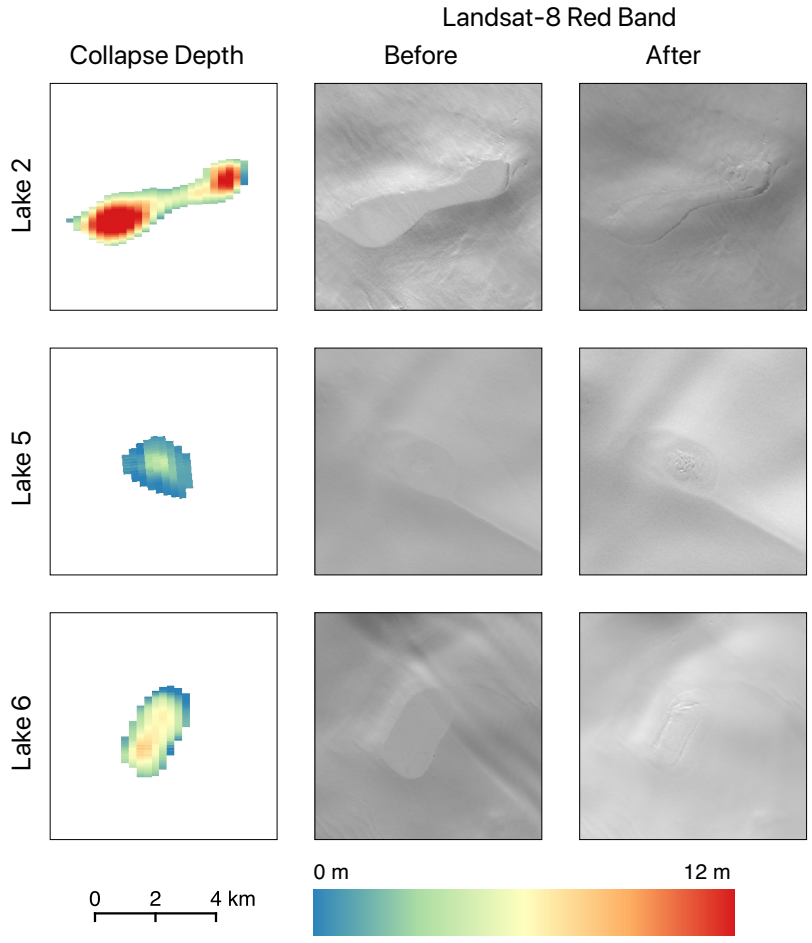

Figure 7. This figure shows the difference results of the photoclinometry analysis beside the before and after images (Landsat-8 Red Band, B4) to illustrate the visible physical changes to the lake lid before and after drainage. The first column of images shows the collapse vertical distance of each pixel. It is the result of interpolating and differencing the pre- and post-drainage topography as mapped out by photoclinometry.

3.3.1 Identifying lake drainage events

230 Identification of a winter lake drainage event using Sentinel-1 data required multiple steps to isolate drainage events from other changes in backscatter. The drainage events identified occurred in lakes of various sizes and locations. If lakes are filtered based only on z-score with no additional filtration done to confirm sustained change, the three seasons analyzed would result in 188, 160, and 221 anomalous lakes for the 2014-2015, 2015-2016, and 2016-2107 winter seasons respectively. For each of these years, retaining only lakes that met the 1.5 z-score threshold and demonstrated no reversal of trend in the first timestep

https://doi.org/10.5194/tc-2020-70
Preprint. Discussion started: 14 May 2020

would result in 75, 60, and 85 lakes, respectively. Reversal was considered to be any change greater than 25% of the magnitude of the anomalous transition occurring either in the previous timestep or in the following three timesteps. Raising this threshold to 30% results in 4 anomalous lakes for each season. Raising the same threshold to 40% results in 10, 7, and 10 lakes for the three seasons. Raising the same threshold again to 50% results in 25, 19, and 21 lakes for the three seasons measured.

Extending the requirement for stability by requiring more consecutive images without reversal would be difficult in most years due to the limited image acquisition over this site. Overall the filtration proved not to be overly sensitive to z-score threshold, as all drained lakes had z-scores over 2 even though the threshold set was 1.5. The criteria used to determine lake drainage events is thought to be conservative and is more likely to have missed drainage events (including false negative ones) than to have found drainage events that were not real (false-positive).

3.3.2 Optical lake mask

As lake delineation using Sentinel-1 backscatter alone is not trivial (Miles et al., 2017; Wangchuk et al., 2019), all change tracking in this study is based on lake outlines generated from Landsat-8 optical imagery. However, in comparing the optically generated masks to the Sentinel-1 backscatter images, the two are often different, typically with the SAR images showing larger lake areas than those from the optical data. This discrepancy may be due to water depths insufficient to meet the $NDWI_{ice}$ threshold set, or may be due to shallow subsurface water below a snow or ice lid. This is most apparent in Lake 6 (Figures 5 and 6, where a low-$NDWI_{ice}$ island appears in the center of the lake, but backscatter measurements remain low in this portion and photoclinometry changes show a caving-in of ice in this area (Figure 5), possibly pointing to this as a floating island of snow with water concealed beneath. Beginning with the $NDWI_{ice}$ mask also results in the splitting of some lakes into multiple disconnected water bodies where parts of the lake are below the threshold. As such, some larger lakes may be filtered out of the study as they appear to be a collection of smaller lakes, and some backscatter tracking is only occurring on partial lakes, where only deeper portions with higher $NDWI_{ice}$ values are included in the lake delineation.

We have used masks in this study created from just a few late-season images to reduce the likelihood of incorporating lakes that drained within the summer into our wintertime lake tracking algorithm. Creating lake masks using a longer time span of images might allow for more complete lake boundaries to be included. By including more summer images, these masks might account for areas of water that are only occasionally seen at the surface but are more often under snow or ice, so especially those at higher elevations. Lake 1, for example, often appears below the 0.25 $NDWI_{ice}$ threshold due to the absence of cloud-free and unfrozen images within a given summer, although the lower backscatter in this area seems to indicate water below.

3.3.3 Sentinel-1 backscatter

While Sentinel-1 backscatter allows for the tracking of lakes that are obscured by the cover of cloud and darkness, it is also limited in what it can observe. Winter lakes are buried beneath an ice lid, generally below snow. The penetration depth of C-band backscatter varies based on the physical properties of the medium through which it passes, especially dependent on moisture, but reaches a maximum of approximately 9 m of depth (Rignot et al., 2001). It is possible that winter lakes exist

https://doi.org/10.5194/tc-2020-70
Preprint. Discussion started: 14 May 2020

below this depth and are missed by the Sentinel-1 backscatter used in this study. This penetration depth is also likely to be insufficient to reach the buried firn aquifers identified in the Greenland Ice Sheet (Forster et al., 2014; Koenig et al., 2014).

Occasionally, images showed large scene-wide departures from typical backscatter values. These images (dated: 03 Feb 2015, 10 Apr 2016, and 16 May 2016) were omitted in this study as they were anomalous although if it were known what caused this phenomenon then perhaps the images could be corrected and used.

Sentinel-1 is also limited in its frequency of available imagery for the same site. While the repeat pass time of Sentinel-1 is at most 6 days when both satellites are included, it is necessary to use imagery from the same relative orbit for greater consistency from image to image, and not all images within each path are acquired. A shorter repeat pass could help more accurately assess the rate of backscatter change and thus gain a better understanding of the nature of these drainage events. For example, no image in Relative Orbit 17 exists between 06 Nov 2016 and 18 Nov 2016, the dates across which we assess Lake 6 to be draining, a 12-day gap in sensing. If additional orbits are included in this analysis, the gap can be reduced to 10 days, but no further.

3.3.4 Drainage water volume

Sentinel-1 backscatter alone does not allow for the estimation of water volumes and therefore water volume changes. The optical satellite data available can be used to estimate the volume, but the optical measurements are limited in their capability to calculate accurately the drained volume. In this study, physically based depth measurements are made for each lake per pixel based on the last available image in the summer before the lake is covered by a frozen lid (Table 1). This calculation provides an estimate of the drained lake volume, assuming that no more water can be drained than is present at the formation of the ice lid. However, these measurements have been shown to underestimate the depth of deep water (Pope et al., 2016; Williamson et al., 2018). Additionally, these measurements occur months prior to the drainage events, and the lake volumes derived from them could be impacted by additional melt filling the lake or freezing of water prior to the drainage event. This study has also set the lake boundary using an $NDWI_{ice}$ threshold of 0.25, which may underestimate the full extent of the lake area. There is also no reliable method of using optical data to measure whether any water remains at the start of the melt season. Images showing the first water visible in the summer after drainage could be showing water remaining in the lake or water transported into the basin from higher elevations. Often cloud-free images are not available until well into the melt season and thus cannot reliably be used as a lower bound to a calculation of water volume difference from the previous autumn.

Photoclinometry results show for each lake a topographical change in the surface shape between the pre- and post- drainage images indicating an elevation drop. However, the depth of caving is greater than the deepest measurement estimated by attenuation-based depth calculations prior to winter. There are also some areas (for example, the northern portion of Lake 2) where shadows exist in the Landsat-8 imagery that would invalidate the reflectance to slope relationship and introduce error into the calculations of the topography for the shaded pixels. While the depth estimation using this technique may be inaccurate in places for the reasons outlined above, the technique confirms that a change in surface topography has occurred. Additionally, the smaller volume estimates for the area-depth technique may be due to the lake depth algorithm underestimating depths beyond a certain threshold (Pope et al, 2016; Williamson et al, 2018) as well as error resulting from differences between the

https://doi.org/10.5194/tc-2020-70
Preprint. Discussion started: 14 May 2020

actual surface topography at the time the Landsat-8 image was taken compared to that in the ArcticDEM. Photoclinometry is potentially a useful method for detecting surface or shallow subsurface lake drainages on ice sheets and ice shelves.

The optical data supports the assertion that the changes in SAR backscatter observed are lake drainage events. The larger lakes in the study, Lakes 2, 5, and 6 all show a significant reduction in lake area in the summer following the winter drainage compared to the previous summer with more than a single summer season needed to regain pre-drainage lake area. This may be due to the opening of a fracture that continues to allow water to drain through the lake bed for some time, similar to that found by Chudley et al. (2019). The smaller lakes did re-fill to their former size in the summer following drainage but changed shape, indicating that the fracture closed up or was advected out of the lake basin prior to the subsequent summer.

3.3.5 Causes and implications of lake drainage

The causes of lake drainage events have been studied extensively (Williamson et al., 2018; Christoffersen et al., 2018). However the observation of winter isolated lake drainages points to the possibility that drainages can occur without increases to lake volume to actively cause hydrofracture or to connect to a nearby moulin to trigger sliding or uplift and passively open a crack. Instead, ice dynamics unrelated to surface hydrology can trigger drainage. The evidence available in this study is insufficient to identify conclusively the cause of these winter lake drainages. Appendix Figure B1 shows the locations of the winter lake drainage events compared to ice speeds derived from MEaSUREs data (Howat, 2017) for the winter periods containing each drainage event. No pattern of lake locations and speeds seems to be visible. In this study, most of the lake drainages occur in isolation - with the exception of the drainages of Lakes 3 and 4, which occur in the same 12-day period. These lakes are separated by a linear distance of 14.9 km. These concurrent drainages support the observations of Christoffersen et al. (2018) of cascade draining or may indicate a larger scale ice movement that triggered both events simultaneously. In the summer after drainage, these small lakes fill to pre-drainage levels, though the footprint of the lake changes, whereas the larger lakes (Lakes 2, 5, and 6) do not reach pre-drainage levels for at least 1-2 years. It is possible that this difference is simply because the larger lakes require more runoff to fill and thus it takes more time to fill them. However, another possible explanation is that the fracture that drained the small lakes was advected out of the lake basin more quickly both because of the smaller basin size and the relatively fast ice velocity in this area (see Appendix Figure B1) and that the larger lakes remain connected to the fractures that drained them for a longer period of time.

4 Conclusions

We have developed an automated method for identifying large, sudden, anomalous and sustained backscatter changes in Sentinel-1 SAR imagery, which we apply to "winter" images collected between October and May spanning three winter seasons. We find six such large, sudden, anomalous and sustained backscatter changes, which are indicative of winter lake drainage events across a study site containing approximately 300 lakes. The events are validated using optical imagery from before and after the winter seasons, which are used to provide estimates of lake volumes associated with the drainages. While these events are rare, they provide conclusive evidence for the first time that lake drainages over winter occur. They are likely

https://doi.org/10.5194/tc-2020-70
Preprint. Discussion started: 14 May 2020

triggered simply by crevasse opening across the lake due to high surface strain rates associated with background winter ice movement. This shows that rapid lake drainage events do not have to be triggered during lake water filling, as has been observed previously for summer events. A full picture of the hydrology of the Greenland Ice Sheet requires observation of surface water on a multi-year and multi-season basis. Identification of the drainage events was achieved by developing a time-series filtering algorithm that may be adapted to identify other hydrological phenomena and behaviour in surface or shallow subsurface water bodies on ice sheets and ice shelves. The algorithm is based on a set of thresholds that were set conservatively to capture only the most obvious incidences of large, anomalous, sudden and sustained backscatter changes and therefore our study is more likely to have underestimated rather than overestimated the number of winter lake drainages (included false negatives rather than false positives). Further study would be required to identify the full range of lake backscatter behaviour through time and what other types of behaviour may indicate. Further work is required to examine whether winter lake drainage occurs in other parts of the ice sheet, in other years, to examine more precisely what the triggering mechanisms are, how basal hydrology and biogeochemistry are affected, and whether winter lake drainage will become more prevalent under future climate warming scenarios.

Data availability. All data used in this study are available publicly through ESA, USGS, and Google Earth Engine.

Appendix A: Appendix A: Photoclinometry process

A1 List of Landsat-8 images used for Photoclinometry

Table A1 of Landsat-8 images were used for the photoclinometry portion of the study (see 2)

Table A1. Landsat-8 images used for photoclinometry process.

Lake	Landsat-8 Scene
Lake 2 Before	LC08 _008012 _20141101
Lake 2 After	LC08 _008012 _20150221
Lake 5 Before	LC08 _008011 _20151104
Lake 5 After	LC08 _008011 _20160428
Lake 6 Before	LC08 _009011 _20161028
Lake 6 After	LC08 _009011 _20170217

https://doi.org/10.5194/tc-2020-70
Preprint. Discussion started: 14 May 2020

A2 Slope vs. Reflectance

Figure A1 show the correlation of slope with reflectance for the non-lake areas of each of the Landsat-8 images used in the photoclinometry section of this study. For each image, a new relationship was established and used to infer the slope of the lake area within that image.

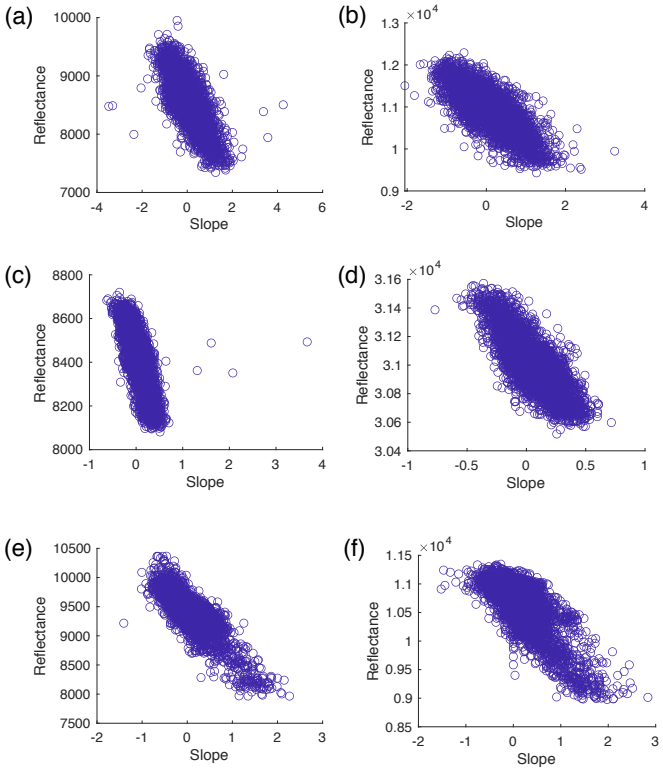

Figure A1. Plots of slope vs. Landsat-8 red band reflectance for areas outside of the lake and buffer zone for each of the Landsat-8 images analyzed for the photoclinometry portion of this study. The plots are laid out as follows: (a) Lake 2 Before, (b) Lake 2 After, (c) Lake 5 Before, (d) Lake 5 after, (e) Lake 6 Before, and (f) Lake 6 After. Images are the same as those in A2

A3 Lake sampling

Figure A2 shows the typical arrangement of the photoclinometry portion of the study. The lake was manually outlined, buffered, and transects were spaced every 250 m and sampled every 30m along transect for each 10 km long transect.

https://doi.org/10.5194/tc-2020-70
Preprint. Discussion started: 14 May 2020

The Cryosphere Discussions
Open Access
EGU

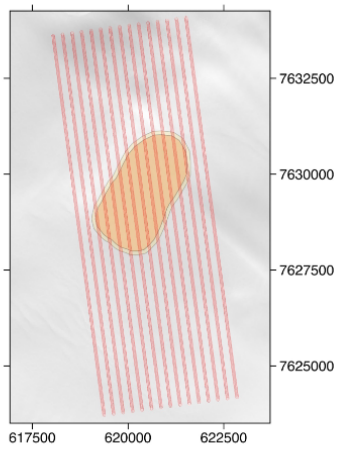

Figure A2. Lake 6 transects for photoclinometry calculations for image on 28 Oct 2016 prior to drainage (red), lake extent (orange) and buffer (yellow). For description of how these features are used in the photoclinometry calculations, see Methods..

Appendix B: Appendix B

Figure B1 presents pixel by pixel ice speeds based on MEaSUREs velocity data (Howat, 2017) for the quarters nearest each of the drainage events.

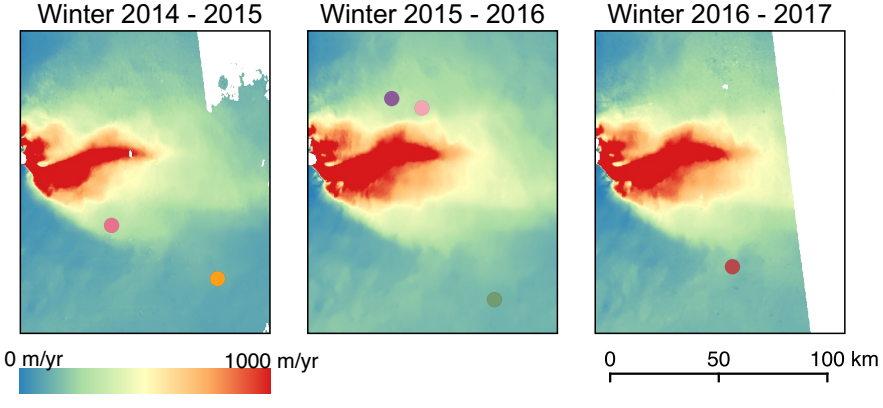

Figure B1. This figure shows the ice speeds for the winter quarter proximate to each of the lake drainages.

https://doi.org/10.5194/tc-2020-70
Preprint. Discussion started: 14 May 2020

Author contributions. Both authors conceived of the work, contributed to the ideas and wrote and edited the paper. CB performed all the analysis and produced all the Figures.

Competing interests. The authors declare no competing interests.

Acknowledgements. CB is funded by the Howard Research Studentship through Sidney Sussex College and the Cambridge Trust. The ArcticDEM was downloaded from Google Earth Engine through the Polar Geospatial Center, University of Minnesota. DEM(s) were created from DigitalGlobe, Inc., imagery and funded under National Science Foundation awards 1043681, 1559691, and 1542736. We thank Marco Tedesco, Neil Arnold, Gareth Rees, Tom Chudley, and Andrew Williamson for useful discussions about various aspects of this work at different stages.

https://doi.org/10.5194/tc-2020-70
Preprint. Discussion started: 14 May 2020


The Cryosphere Discussions
Open Access
EGU

References

Alley, R., Dupont, T., Parizek, B., and Anandakrishnan, S.: Access of surface meltwater to beds of sub-freezing glaciers: preliminary insights, Annals of Glaciology, 40, 8–14, 2005.

Arnold, N., Banwell, A., and Willis, I.: High-resolution modelling of the seasonal evolution of surface water storage on the Greenland Ice Sheet, The Cryosphere, 8, 1149–1160, 2014.

Banwell, A., Arnold, N., Willis, I., Tedesco, M., and Ahlstrøm, A.: Modeling supraglacial water routing and lake filling on the Greenland Ice Sheet, Journal of Geophysical Research: Earth Surface, 117, 2012.

Banwell, A., Hewitt, I., Willis, I., and Arnold, N.: Moulin density controls drainage development beneath the Greenland ice sheet, Journal of Geophysical Research: Earth Surface, 121, 2248–2269, 2016.

Bartholomew, I., Nienow, P., Mair, D., Hubbard, A., King, M., and Sole, A.: Seasonal evolution of subglacial drainage and acceleration in a Greenland outlet glacier, Nature Geoscience, 3, 408, 2010.

Bartholomew, I., Nienow, P., Sole, A., Mair, D., Cowton, T., Palmer, S., and Wadham, J.: Supraglacial forcing of subglacial drainage in the ablation zone of the Greenland ice sheet, Geophysical Research Letters, 38, 2011.

Box, J. and Ski, K.: Remote sounding of Greenland supraglacial melt lakes: implications for subglacial hydraulics, Journal of glaciology, 53, 257–265, 2007.

Christoffersen, P., Bougamont, M., Hubbard, A., Doyle, S., Grigsby, S., and Pettersson, R.: Cascading lake drainage on the Greenland Ice Sheet triggered by tensile shock and fracture, Nature communications, 9, 1064, 2018.

Chudley, T., Christoffersen, P., Doyle, S., Bougamont, M., Schoonman, C., Hubbard, B., and James, M.: Supraglacial lake drainage at a fast-flowing Greenlandic outlet glacier, Proceedings of the National Academy of Sciences, 2019.

Clason, C., Mair, D., Nienow, P., Bartholomew, I., Sole, A., Palmer, S., and Schwanghart, W.: Modelling the transfer of supraglacial meltwater to the bed of Leverett Glacier, Southwest Greenland, The Cryosphere, 9, 123–138, 2015.

Das, S., Joughin, I., Behn, M., Howat, I., King, M., Lizarralde, D., and Bhatia, M.: Fracture propagation to the base of the Greenland Ice Sheet during supraglacial lake drainage, Science, 320, 778–781, 2008.

Dieser, M., Broemsen, E., Cameron, K., King, G., Achberger, A., Choquette, K., Hagedorn, B., Sletten, R., Junge, K., and Christner, B.: Molecular and biogeochemical evidence for methane cycling beneath the western margin of the Greenland Ice Sheet, The ISME journal, 8, 2305, 2014.

Dow, C., Kulessa, B., Rutt, I., Tsai, V., Pimentel, S., Doyle, S., Van As, D., Lindbäck, K., Pettersson, R., Jones, G., et al.: Modeling of subglacial hydrological development following rapid supraglacial lake drainage, Journal of Geophysical Research: Earth Surface, 120, 1127–1147, 2015.

Doyle, S., Hubbard, A., Dow, C., Jones, G., Fitzpatrick, A. W., Gusmeroli, A., Kulessa, B., Lindback, K., Pettersson, R., and Box, J.: Ice tectonic deformation during the rapid in situ drainage of a supraglacial lake on the Greenland Ice Sheet., Cryosphere, 7, 129–140, 2013.

Forster, R., Box, J., Van Den Broeke, M., Miège, C., Burgess, E., Van Angelen, J., Lenaerts, J., Koenig, L., Paden, J., Lewis, C., et al.: Extensive liquid meltwater storage in firn within the Greenland ice sheet, Nature Geoscience, 7, 95–98, 2014.

Gorelick, N., Hancher, M., Dixon, M., Ilyushchenko, S., Thau, D., and Moore, R.: Google Earth Engine: Planetary-scale geospatial analysis for everyone, Remote Sensing of Environment, 202, 18–27, 2017.

Hawkings, J., Wadham, J., Tranter, M., Telling, J., Bagshaw, E., Beaton, A., Simmons, S., Chandler, D., Tedstone, A., and Nienow, P.: The Greenland Ice Sheet as a hot spot of phosphorus weathering and export in the Arctic, Global Biogeochemical Cycles, 30, 191–210, 2016.

https://doi.org/10.5194/tc-2020-70
Preprint. Discussion started: 14 May 2020

Hewitt, I.: Seasonal changes in ice sheet motion due to melt water lubrication, Earth and Planetary Science Letters, 371, 16–25, 2013.

Hoffman, M., Catania, G., Neumann, T., Andrews, L., and Rumrill, J.: Links between acceleration, melting, and supraglacial lake drainage of the western Greenland Ice Sheet, Journal of Geophysical Research: Earth Surface, 116, 2011.

Hoffman, M., Perego, M., Andrews, L., Price, S., Neumann, T., Johnson, J., Catania, G., and Lüthi, M.: Widespread moulin formation during supraglacial lake drainages in Greenland, Geophysical Research Letters, 45, 778–788, 2018.

Howat, I.: MEaSUREs Greenland Ice Velocity: Selected Glacier Site Velocity Maps from Optical Images, Version 2, NASA National Snow and Ice Data Center Distributed Active Archive Center, Boulder, Colorado, 2017.

Koenig, L., Miège, C., Forster, R., and Brucker, L.: Initial in situ measurements of perennial meltwater storage in the Greenland firn aquifer, Geophysical Research Letters, 41, 81–85, 2014.

Koenig, L., Lampkin, D., Montgomery, L., Hamilton, S., Turrin, J., Joseph, C., Moutsafa, S., Panzer, B., Casey, K., Paden, J., et al.: Winter-time storage of water in buried supraglacial lakes across the Greenland Ice Sheet, The Cryosphere, 9, 1333–1342, 2015.

Koziol, C., Arnold, N., Pope, A., and Colgan, W.: Quantifying supraglacial meltwater pathways in the Paakitsoq region, West Greenland, Journal of Glaciology, 63, 464–476, 2017.

Krawczynski, M., Behn, M., Das, S., and Joughin, I.: Constraints on the lake volume required for hydro-fracture through ice sheets, Geophysical Research Letters, 36, 2009.

Lamarche-Gagnon, G., Wadham, J., Lollar, B., Arndt, S., Fietzek, P., Beaton, A., Tedstone, A., Telling, J., Bagshaw, E., Hawkings, J., et al.: Greenland melt drives continuous export of methane from the ice-sheet bed, Nature, 565, 73–77, 2019.

Law, R., Arnold, N., Benedek, C., Banwell, A., Willis, I., and Tedesco, M.: Over-winter persistence of supraglacial lakes on the Greenland Ice Sheet: results and insights from a new model, Journal of Glaciology, X, XXXX–XXXX, forthcoming 2020.

Leeson, A., Shepherd, A .and Palmer, S., Sundal, A., and Fettweis, X.: Simulating the growth of supraglacial lakes at the western margin of the Greenland ice sheet., The cryosphere., 6, 1077–1086, 2012.

Leeson, A., Shepherd, A., Sundal, A., Johansson, A., Selmes, N., Briggs, K., Hogg, A., and Fettweis, X.: A comparison of supraglacial lake observations derived from MODIS imagery at the western margin of the Greenland ice sheet, Journal of Glaciology, 59, 1179–1188, 2013.

Liang, Y., Colgan, W., Lv, Q., Steffen, K., Abdalati, W., Stroeve, J., Gallaher, D., and Bayou, N.: A decadal investigation of supraglacial lakes in West Greenland using a fully automatic detection and tracking algorithm, Remote Sensing of Environment, 123, 127–138, 2012.

Lüthje, M., Pedersen, L., Reeh, N., and Greuell, W.: Modelling the evolution of supraglacial lakes on the West Greenland ice-sheet margin, Journal of Glaciology, 52, 608–618, 2006.

McMillan, M., Nienow, P., Shepherd, A., Benham, T., and Sole, A.: Seasonal evolution of supra-glacial lakes on the Greenland Ice Sheet, Earth and Planetary Science Letters, 262, 484–492, 2007.

Miles, K., Willis, I., Benedek, C., Williamson, A., and Tedesco, M.: Toward monitoring surface and subsurface lakes on the Greenland ice sheet using Sentinel-1 SAR and Landsat-8 OLI imagery, Frontiers in Earth Science, 5, 58, 2017.

Moussavi, M., Abdalati, W., Pope, A., Scambos, T., Tedesco, M., MacFerrin, M., and Grigsby, S.: Derivation and validation of supraglacial lake volumes on the Greenland Ice Sheet from high-resolution satellite imagery, Remote Sensing of Environment, 183, 294–303, 2016.

Musilova, M., Tranter, M., Wadham, J., Telling, J., Tedstone, A., and Anesio, A.: Microbially driven export of labile organic carbon from the Greenland ice sheet, Nature Geoscience, 10, 360, 2017.

Pimentel, S. and Flowers, G.: A numerical study of hydrologically driven glacier dynamics and subglacial flooding, Proceedings of the Royal Society A: Mathematical, Physical and Engineering Sciences, 467, 537–558, 2010.

https://doi.org/10.5194/tc-2020-70
Preprint. Discussion started: 14 May 2020

Pope, A., Willis, I., Rees, W., Arnold, N., and Pálsson, F.: Combining airborne lidar and Landsat ETM+ data with photoclinometry to produce a digital elevation model for Langjökull, Iceland, International journal of remote sensing, 34, 1005–1025, 2013.

Pope, A., Scambos, T.A .and Moussavi, M., Tedesco, M., Willis, M., Shean, D., and Grigsby, S.: Estimating supraglacial lake depth in West Greenland using Landsat 8 and comparison with other multispectral methods, The Cryosphere, 10, 15, 2016.

Rennermalm, A., Smith, L., Chu, V., Box, J., Forster, R., and Van den Broeke, M.: Evidence of meltwater retention within the Greenland ice sheet, The Cryosphere Discuss, 6, 3369–3396, 2012.

Rignot, E., Echelmeyer, K., and Krabill, W.: Penetration depth of interferometric synthetic-aperture radar signals in snow and ice, Geophysical Research Letters, 28, 3501–3504, 2001.

Russell, A.: Supraglacial lake drainage near Sendre Strømjjord, Greenland, Journal of Glaciology, 39, 431–433, 1993.

Schoof, C.: Ice-sheet acceleration driven by melt supply variability, Nature, 468, 803, 2010.

Selmes, N., Murray, T., and James, T.: Fast draining lakes on the Greenland Ice Sheet, Geophysical Research Letters, 38, 2011.

Selmes, N., Murray, T., and James, T.: Characterizing supraglacial lake drainage and freezing on the Greenland Ice Sheet, The Cryosphere Discussions, 7, 475–505, 2013.

Shade, A., Peter, H., Allison, S., Baho, D., Berga, M., Bürgmann, H., Huber, D., Langenheder, S., Lennon, J., Martiny, J., et al.: Fundamentals of microbial community resistance and resilience, Frontiers in microbiology, 3, 417, 2012.

Sneed, W. and Hamilton, G.: Evolution of melt pond volume on the surface of the Greenland Ice Sheet, Geophysical Research Letters, 34, 2007.

Stevens, L., Behn, M., McGuire, J., Das, S., Joughin, I., Herring, T., Shean, D., and King, M.: Greenland supraglacial lake drainages triggered by hydrologically induced basal slip, Nature, 522, 73, 2015.

Tedesco, M., Lüthje, M., Steffen, K., Steiner, N., Fettweis, X., Willis, I., Bayou, N., and Banwell, A.: Measurement and modeling of ablation of the bottom of supraglacial lakes in western Greenland, Geophysical Research Letters, 39, 2012.

Tedesco, M., Willis, I., Hoffman, M., Banwell, A., Alexander, P., and Arnold, N.: Ice dynamic response to two modes of surface lake drainage on the Greenland ice sheet, Environmental Research Letters, 8, 034 007, 2013.

Tsai, V. and Rice, J.: A model for turbulent hydraulic fracture and application to crack propagation at glacier beds, Journal of Geophysical Research: Earth Surface, 115, 2010.

van der Veen, C.: Fracture propagation as means of rapidly transferring surface meltwater to the base of glaciers, Geophysical Research Letters, 34, 2007.

Wadham, J., Tranter, M., Skidmore, M., Hodson, A., Priscu, J., Lyons, W., Sharp, M., Wynn, P., and Jackson, M.: Biogeochemical weathering under ice: size matters, Global Biogeochemical Cycles, 24, 2010.

Wadham, J., Hawkings, J., Telling, J., Chandler, D., Alcock, J., Lawson, E., Kaur, P., Bagshaw, E., Tranter, M., Tedstone, A., et al.: Sources, cycling and export of nitrogen on the Greenland Ice Sheet, Biogeosciences Discussions, 2016.

Wangchuk, S., Bolch, T., and Zawadzki, J.: Towards automated mapping and monitoring of potentially dangerous glacial lakes in Bhutan Himalaya using Sentinel-1 Synthetic Aperture Radar data, International journal of remote sensing, 40, 4642–4667, 2019.

Werder, M., Hewitt, I., Schoof, C., and Flowers, G.: Modeling channelized and distributed subglacial drainage in two dimensions, Journal of Geophysical Research: Earth Surface, 118, 2140–2158, 2013.

White, A., Mueller, D., and Copland, L.: Reconstructing hydrographic change in Petersen Bay, Ellesmere Island, Canada, inferred from SAR imagery, Remote Sensing of Environment, 165, 1–13, 2015.

https://doi.org/10.5194/tc-2020-70
Preprint. Discussion started: 14 May 2020

Williamson, A., Arnold, N., Banwell, A., and Willis, I.: A Fully Automated Supraglacial lake area and volume Tracking ("FAST") algorithm: Development and application using MODIS imagery of West Greenland, Remote Sensing of Environment, 196, 113–133, 2017.

Williamson, A., Banwell, A., Willis, I., and Arnold, N.: Remote sensing of supraglacial lakes in Greenland using a combined Sentinel-2 and Landsat-8 record, The Cryosphere, 12, 3045–3065, 2018.

Yang, K. and Smith, L.: Supraglacial streams on the Greenland Ice Sheet delineated from combined spectral–shape information in high-resolution satellite imagery, IEEE Geoscience and Remote Sensing Letters, 10, 801–805, 2012.